J. Iron Steel Res. Int.
https://doi.org/10.1007/s42243-024-01249-8

ORIGINAL PAPER

Iron recovery and dephosphorization behaviors from high-phosphorus oolitic hematite by gas-based direct reduction and magnetic separation

Fang Liu[1,2] · Yi-chi Zhang[3] · Wang Zeng[1] · Jun Ni[2] · Yun-peng Si[1] · Heng Zhou[1,2] · Tian-xiang Zhang[3] · Sheng-li Wu[1,2] · Ming-yin Kou[1,2]

Received: 5 January 2024 / Revised: 6 February 2024 / Accepted: 7 March 2024
© China Iron and Steel Research Institute Group Co., Ltd. 2024

Abstract
With the depletion of high-quality iron ore resources, high-phosphorus oolitic hematite (HPOH) has attracted great attention due to its large reserve and relatively high iron content. However, HPOH is very difficult to be used in ironmaking process due to its special structure. A two-step method of gas-based direct reduction and magnetic separation was thus proposed to recover iron and reduce phosphorus. The results showed that the powdery reduced iron produced contained 92.31% iron and 0.1% phosphorus, and the iron recovery was 92.65% under optimum reduction condition, which is suitable for following steelmaking. The apatite will be reduced under long reduction time and a large reducing gas flow rate, resulting in more phosphorus found in the metallic iron. Increasing the hydrogen–carbon ratio will inhibit the formation and growth of iron particles and prevent the breakage of oolitic structure. Careful adjustment of reduction temperature is recommended as it affects the oolitic structure and reduction.

Keywords High-phosphorus oolitic hematite · Iron recovery · Dephosphorization · Gas-based direct reduction · Magnetic separation

1 Introduction

Due to the continuous development of iron and steel industry, high-quality iron ore is rapidly decreasing year after year. Therefore, some low-grade iron ores turn out to be alternative options of steel companies [1, 2]. Among them, high-phosphorus oolitic hematite (HPOH) is a competitive choice since it has a relatively high iron content (average 52%) and a large reserve of 3.72×10^9 t, accounting for about 7% of the total iron ore resources in China [3, 4]. However, HPOH has high phosphorus content and a unique small-particle oolitic structure, which makes it very difficult to be separate phosphorus and iron oxides [5–7]. Therefore, how to decrease phosphorus and recover iron from HPOH is the most challenging factor of utilizing HPOH [8, 9].

Various processes have been developed for the utilization of HPOH, primarily encompassing mineral separation, leaching, and magnetization roasting–magnetic separation [10–12]. For the mineral separation, Yehia et al. [13] used fungal cellulase to enhance the separation of apatite and hematite in the flotation process of HPOH at pH of 10. The use of oleate and cellulase reduced the phosphorus content in natural HPOH from 0.84% to 0.19%, but the iron recovery was only 67.85%. This method is difficult to separate iron and phosphorus, and the iron loss is large. The leaching method can efficiently remove phosphorus by dissolving phosphorus-bearing gangue minerals (mainly apatite) in the ore. Zhang et al. [14] obtained a product with

✉ Heng Zhou
zhouheng@ustb.edu.cn

✉ Ming-yin Kou
koumingyin@ustb.edu.cn

[1] State Key Laboratory of Advanced Metallurgy, University of Science and Technology Beijing, Beijing 100083, China

[2] School of Metallurgical and Ecological Engineering, University of Science and Technology Beijing, Beijing 100083, China

[3] School of Automation and Electrical Engineering, University of Science and Technology Beijing, Beijing 100083, China

Published online: 30 May 2024

TFe (total iron) of 48.80% and a phosphorus content of 0.73% based on alkaline leaching of HPOH, and the phosphorus content of leached ore is as low as 0.10%. However, this approach does not enhance TFe and may lead to environmental contamination. As for magnetization roasting–magnetic separation, it is a method to reduce weak magnetic iron minerals (Fe_2O_3) to strong magnetic magnetite (Fe_3O_4) and magnetic hematite (Y-Fe_2O_3) and then use low magnetic separation to separate iron minerals and gangue minerals. By analyzing the reduction mechanism of iron oxides, Zhang et al. [15] conducted magnetization roasting–magnetic separation–reverse flotation separation process of HPOH with TFe of 47.71% and phosphorus content of 0.874% and obtained an iron concentrate with TFe of 61.78% and phosphorus content of 0.23%. However, this process has high iron loss and low dephosphorization efficiency, which is not an excellent treatment method. These traditional separation technologies are difficult to obtain products with high TFe and low phosphorus content. They have failed to efficiently recover iron and dephosphorization, and it is necessary to explore a better process.

Recently, the reduction–magnetic separation process was proposed as a new direction for the utilization of HPOH [16–18]. This process includes roasting reduction and grinding magnetic separation. It can simultaneously achieve iron recovery and dephosphorization. In addition, resource utilization is efficient and the method is simple. Generally, the TFe content of the obtained product is more than 90% and the phosphorus content is no more than 0.1% [19, 20], which is a high-quality steelmaking raw material. Numerous researchers have extensively investigated the kinetics [21], thermodynamics [22], effects of additives [23], and the behaviors of iron and phosphorus [15] in the reduction and dephosphorization of HPOH. By controlling the reduction atmosphere and optimizing the roasting condition without adding a dephosphorization agent, Wu et al. [24] obtained powdery reduced iron with TFe of 92.77% and phosphorus content of 0.09%. However, the iron recovery was only 68.70%. Besides, those processing methods are coal-based and therefore require high temperature, which generate significant energy consumption and carbon emissions.

Compared with the coal-based reduction, gas-based reduction has less pollution and lower temperature. Therefore, Wu et al. [25] proposed a oxidation roasting–gas-based reduction and magnetic separation process to obtain powdery reduced iron with TFe of 91.37%, phosphorus content of 0.14% and iron recovery of 92.81%. However, this complex process requires roasting to destroy the oolitic structure, without taking into account the effect of the ratio of reducing gas.

Therefore, in the present study, we propose a gas-based direct reduction–magnetic separation process to conduct reduction and dephosphorization experiments on HPOH. The process flow is short. The reduction and destruction of oolitic structure can be carried out simultaneously. After studying the influence of reducing gas flow rate, reduction time, hydrogen–carbon ratio and temperature on reduction behaviors, the optimum conditions for dephosphorization and iron recovery in the reduction process of HPOH were clarified, providing a new idea for its utilization.

2 Experimental

2.1 Materials

The HPOH used in this study was taken from Wushan, Chongqing, China. The reducing gases used in the experiment were CO and H_2, and the dephosphorization agent was analytically pure $CaCO_3$. The results of chemical detection of ore samples are shown in Table 1. The TFe and phosphorus contents were determined employing the methodologies specified in GB/T 6730.65–2009 and GB/T 6730.18–2006, respectively. The crystal phases and microstructures were measured by X-ray diffraction (XRD, STADIVARI, STOE, Germany) and scanning electron microscopy–energy dispersive spectrometry (SEM–EDS, MLA250, FEI Quanta, USA).

Figure 1 shows the microstructure of HPOH, and the obvious oolitic structure can be seen. Figure 2 is the XRD pattern of HPOH and it can be seen that the main minerals in the raw ore are hematite, apatite, quartz and chlorite. Tables 2 and 3 are the occurrence states of iron and phosphorus, respectively. From Table 2, it can be seen that iron in the raw ore is mainly present in hematite, accounting for 96.21% of total iron. A small amount of iron is present in chlorite, accounting for 3.53% of total iron. Table 3 reveals that the phosphorus in the raw ore is primarily present in the apatite, accounting for approximately 96.21% of the total phosphorus. A small amount of phosphorus is also found in the chlorite, contributing 3.59% of the total phosphorus content.

2.2 Experimental procedure

The experimental process is shown in Fig. 3. Firstly, the ore powder was pulverized to a size of -1 mm (0.5−1 mm: 30.3%, 0.25–0.5 mm: 29.9%, 0.15–0.25 mm: 18.8%, $\leq$ 0.15 mm: 21%). Secondly, it was mixed with 8 wt.% water and a certain amount of $CaCO_3$, producing green pellets with a diameter ranging from 12.5 to 15.0 mm. Thirdly, the green pellets were dried at 105 °C for 12 h. Fourthly, six to seven pellet samples were put in a

Table 1 Main chemical composition of high-phosphorus oolitic hematite (wt.%)

Component	TFe	SiO_2	Al_2O_3	CaO	MgO	MnO	P	S	K	Na
Content	50.49	11.21	5.23	5.05	0.85	0.26	1.35	0.06	0.34	0.18

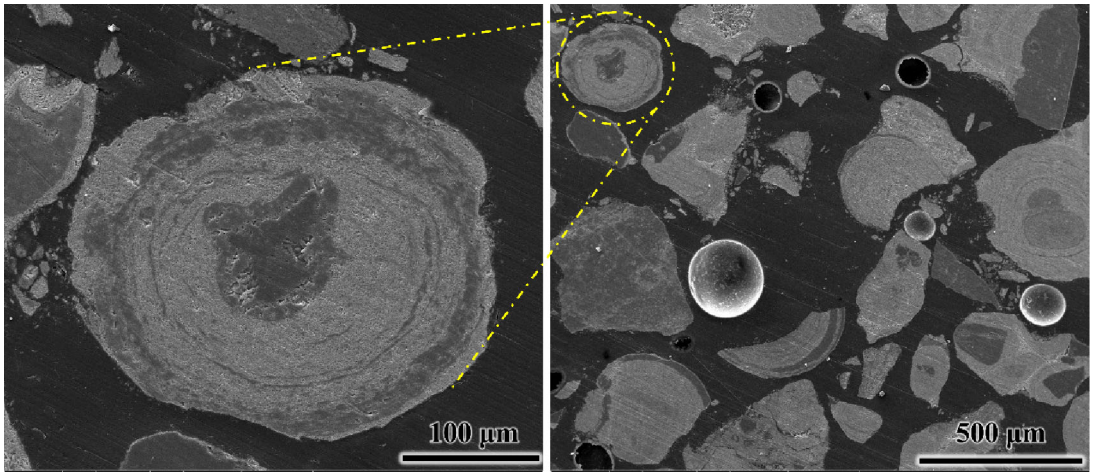

Fig. 1 Micromorphology of HPOH

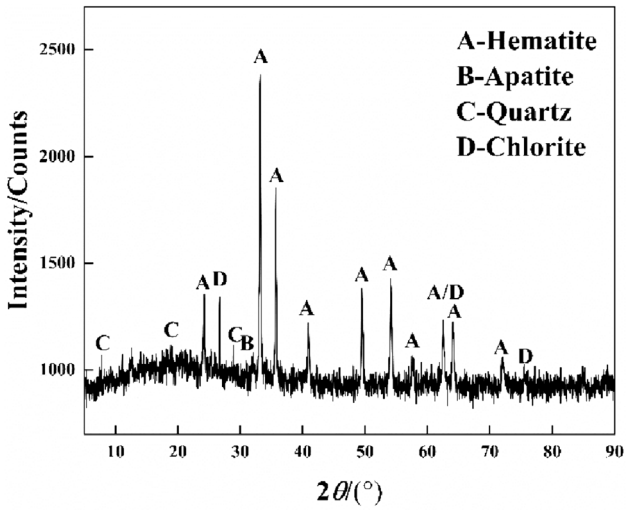

Fig. 2 XRD pattern of HPOH. 2θ—Diffraction angle

metal basket and placed in a reduction furnace following the temperature and gas profiles in Fig. 4. A protective gas flow of 2 L/min of N_2 was performed in the heating stage. It was switched to the reducing gas (including 30% N_2 as protecting gas) once the target temperature was reached. It was changed to a N_2 flow of 2 L/min as protecting gas after the reduction in the cooling stage. Fifthly, the reduced and cooled samples were taken out from the furnace. They were pulverized to a size of − 1 mm, followed by a two-step process of grinding and magnetic separation. The first grinding was 30 min at 140 kA/m magnetic field intensity, followed by a second grinding for 30 min at 120 kA/m magnetic field intensity. The grinding concentration was 67% (12 g sample and 6 g water). The rotation speed of the grinding tank was 289 r/min. At last, the obtained material after grinding and magnetic separation was dehydrated. The final product was referred as powdery reduced iron.

Table 2 Main occurrence minerals of Fe in ore (wt.%)

Mineral phase	Hematite	Chlorite	Apatite	Quartz	Dolomite	Calcite	Others	Total
Mineral content	80.46	7.04	6.53	4.41	0.65	0.13	0.78	100.00
Fe content	62.07	26.03	1.63	0.21	2.53	–	–	–
Fe distribution	96.21	3.53	0.21	0.02	0.03	–	–	100.00

Table 3 Main occurrence minerals of P in ore (wt.%)

Mineral phase	Apatite	Chlorite	Quartz	Hematite	Dolomite	Calcite	Others	Total
Mineral content	6.53	7.04	4.41	80.46	0.65	0.13	0.78	100.00
P content	16.76	0.58	0.05	–	–	–	–	–
P distribution	96.21	3.59	0.19	–	–	–	–	100.00

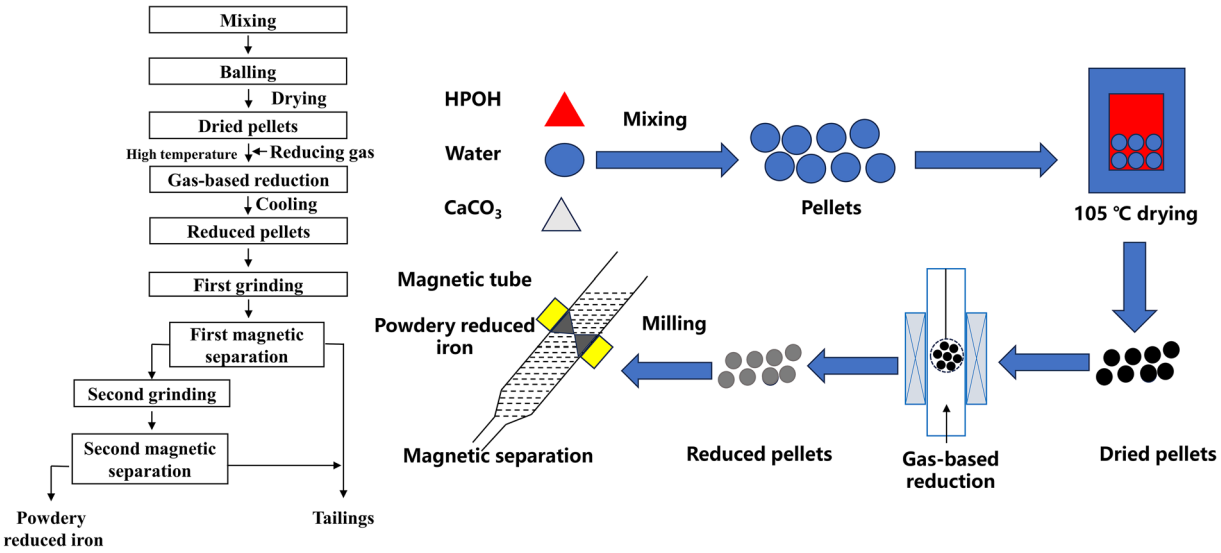

Fig. 3 Flow chart and schematic diagram of experimental process

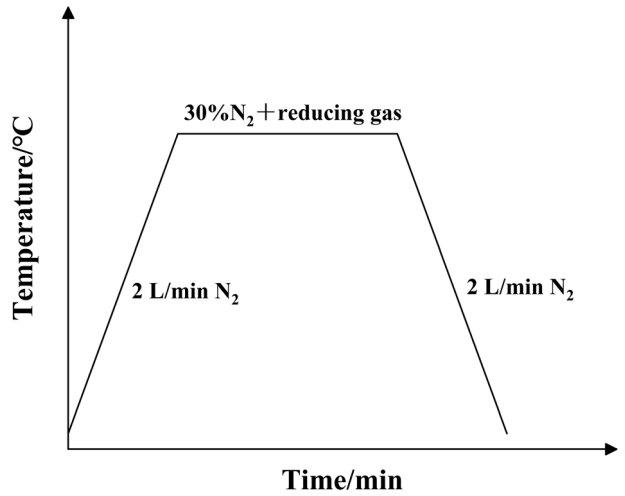

Fig. 4 Reduction process diagram

The main evaluation parameters in this study include TFe, phosphorus content, and iron recovery (η). The equation for calculating the iron recovery is as follows:

$$\eta = \frac{m_1 \times \beta_1}{m_0 \times \beta_0} \quad (1)$$

where m_1 is the mass of the powdery reduced iron, g; m_0 is the mass of the HPOH, g; β_1 is the TFe of the powdery reduced iron, %; and β_0 is the TFe of the HPOH, %.

3 Results and discussion

In order to study the reduction characteristics of HPOH under different conditions, the effects of reducing gas flow rate, reduction time, hydrogen–carbon ratio and temperature were studied in detail. The investigated parameters are shown in Table 4.

Table 4 Parameters used in present work

Parameter	Value
Reducing gas flow rate/(L min^{-1})	3, 4, 5, 6, 7
Reduction time/h	0.5, 1, 2, 3, 4
Hydrogen–carbon ratio	0:1 (CO), 1:3, 1:1, 3:1, 1:0 (H_2)
Reduction temperature/°C	1000, 1050, 1100, 1150

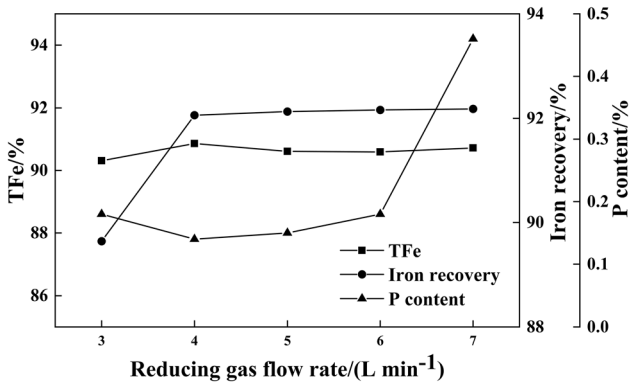

Fig. 5 Effect of reducing gas flow rate on separation indices

3.1 Effect of reducing gas flow rate

Gas-based reduction is a process that is influenced by the flow rate of the reducing gas, which affects not only the reduction of iron but also the conversion behaviors of phosphorus minerals [25]. The effects of reducing gas flow rate on various indicators of powdery reduced iron were explored under the conditions of reduction temperature of 1100 °C, reduction time of 2 h, reducing gas of CO, and $CaCO_3$ addition of 25%. The results are shown in Fig. 5.

The iron recovery increases first and then remains unchanged with the increase in reducing gas flow rate. Gas flow rate has little effect on TFe, which stays within the range of 90%–91%. When the flow rate of reducing gas increases, the phosphorus content decreases to its minimum of 0.14% at the flow rate of 4 L/min and then increases gradually.

The reason for the increase in iron recovery may be that iron particles gather together with an increase in the reducing gas flow rate. The recovery of large iron particles is easier during the process of grinding and magnetic separation. It can be seen from Fig. 6 that when the

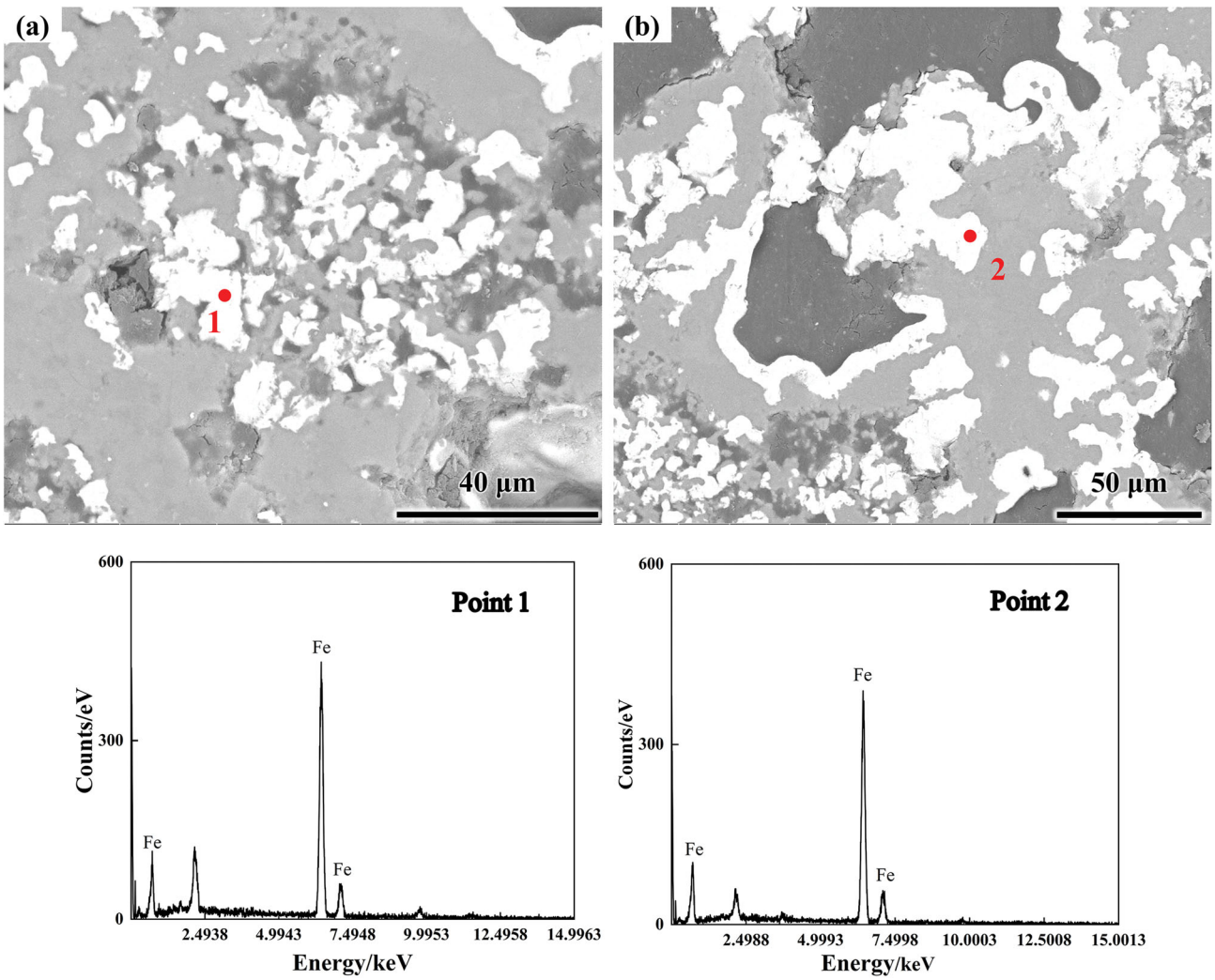

Fig. 6 Microscopic results of reduced pellets at reducing gas flow rate of 3 L/min (**a**) and 4 L/min (**b**)

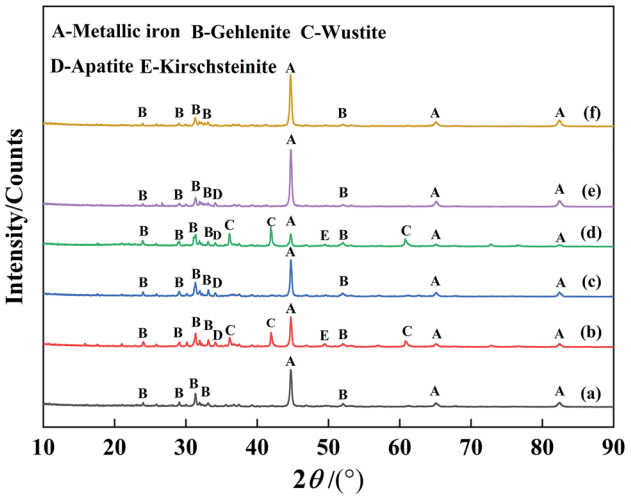

Fig. 7 XRD pattern of reduced pellets. **a** Reducing gas flow rate of 6 L/min; **b** reduction time of 0.5 h; **c** reduction time of 1 h, reduction temperature of 1100 °C; **d** reduction temperature of 1150 °C; **e** hydrogen–carbon ratio of 1:0; **f** hydrogen–carbon ratio of 1:1

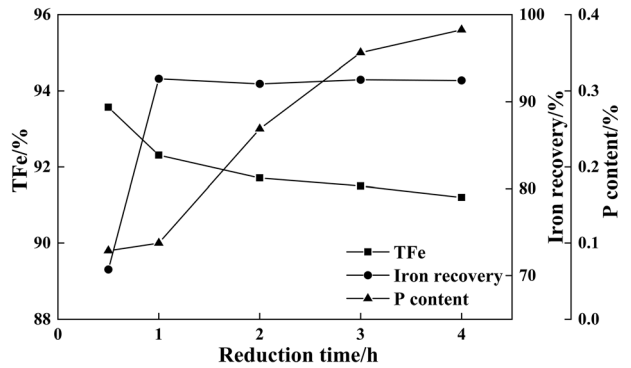

Fig. 8 Effects of reduction time on separation indices

reduction gas flow rate is 4 L/min, the iron particles size reaches 20 μm. Further increase in iron particles has little effect on the iron recovery, resulting in a small change in the iron recovery when the reducing gas flow rate continues to increase.

The reason for the decrease in the phosphorus content may be that the iron particle grows up with the increase in the reducing gas flow rate. This can be proved by Fig. 6, where the white, light gray and dark gray areas are metallic iron phase, gangue phase and epoxy resin, respectively. It can be found that when the reducing gas flow rate is 4 L/min, the iron particles size is larger than that at 3 L/min. The growth of iron particles makes the boundary between iron particles and gangue more obvious, which is beneficial to the separation of iron and phosphorus in the magnetic separation process. The reason for the increase in the phosphorus content may be that some apatite is reduced to P_2 with the increase in the reducing gas flow rate. This can be explained by Fig. 7a. When the flow rate of reducing gas is 7 L/min, the apatite diffraction peak disappeared, indicating that the reduction of apatite and the reaction of P_2 with metallic iron may occur via reactions (2) and (3).

$$2Ca_3(PO_4)_2 + 10CO(g) + 3SiO_2 + 3Al_2O_3 = 10CO_2 + 2P_2(g) + 3Ca_2Al_2SiO_7 \quad (2)$$

$$6Fe + P_2 = 2Fe_3P \quad (3)$$

Considering the effect of reduction gas flow rate on iron reduction and dephosphorization, the optimal reduction gas flow rate is 4 L/min.

3.2 Effect of reduction time

This section investigated the effects of reduction time on various indicators of powder reduced iron. The fixed parameters are reducing gas flow rate of 4 L/min, CO as the reducing gas, and 25% $CaCO_3$ addition at 1100 °C. The results are presented in Fig. 8.

The iron recovery increases to its maximum of 92.65% at the reduction time of 1 h from 70.71% at 0.5 h and almost does not change as the reduction time increases. TFe decreases sharply with reduction time increasing from 0.5 to 1 h and then decreases gradually as the reduction time increases. The phosphorus content increased rapidly with the increase in the reduction time.

The iron mineral is not completely reduced, leading to the low iron recovery, when the reduction time is 0.5 h. This can be proved by Fig. 7b, c. It can be found that the diffraction peaks of wustite and kirschsteinite exist when the reduction time is 0.5 h, and they disappear at 1 h, indicating that the iron minerals are completely reduced to metallic iron. TFe is the highest when the reduction time is 0.5 h, which may be due to that the iron minerals without oolitic structure are reduced to metallic iron particles earlier when the reduction time is insufficient. These iron particles can be easily separated and recovered in grinding magnetic separation because of the simple distribution with gangue. And this is also the reason for the low phosphorus content when the reduction time is 0.5 h. The reason for the slow decrease of TFe may be that the iron particles become larger with the increase in reduction time. This can be explained by Fig. 9. The iron particles obtained after a 4 h reduction exhibit a significantly larger size compared to those obtained after a 1 h reduction. Some gangue materials are wrapped with iron particles, making it challenging to separate the iron particles from the gangues.

The reason for the increase in phosphorus content may be the reduction of apatite and the growth of iron particles, when the reduction time increases from 1 to 4 h. Comparing Fig. 9a and b, it can be found that iron at point 4 contains phosphorus while point 1 contains no phosphorus,

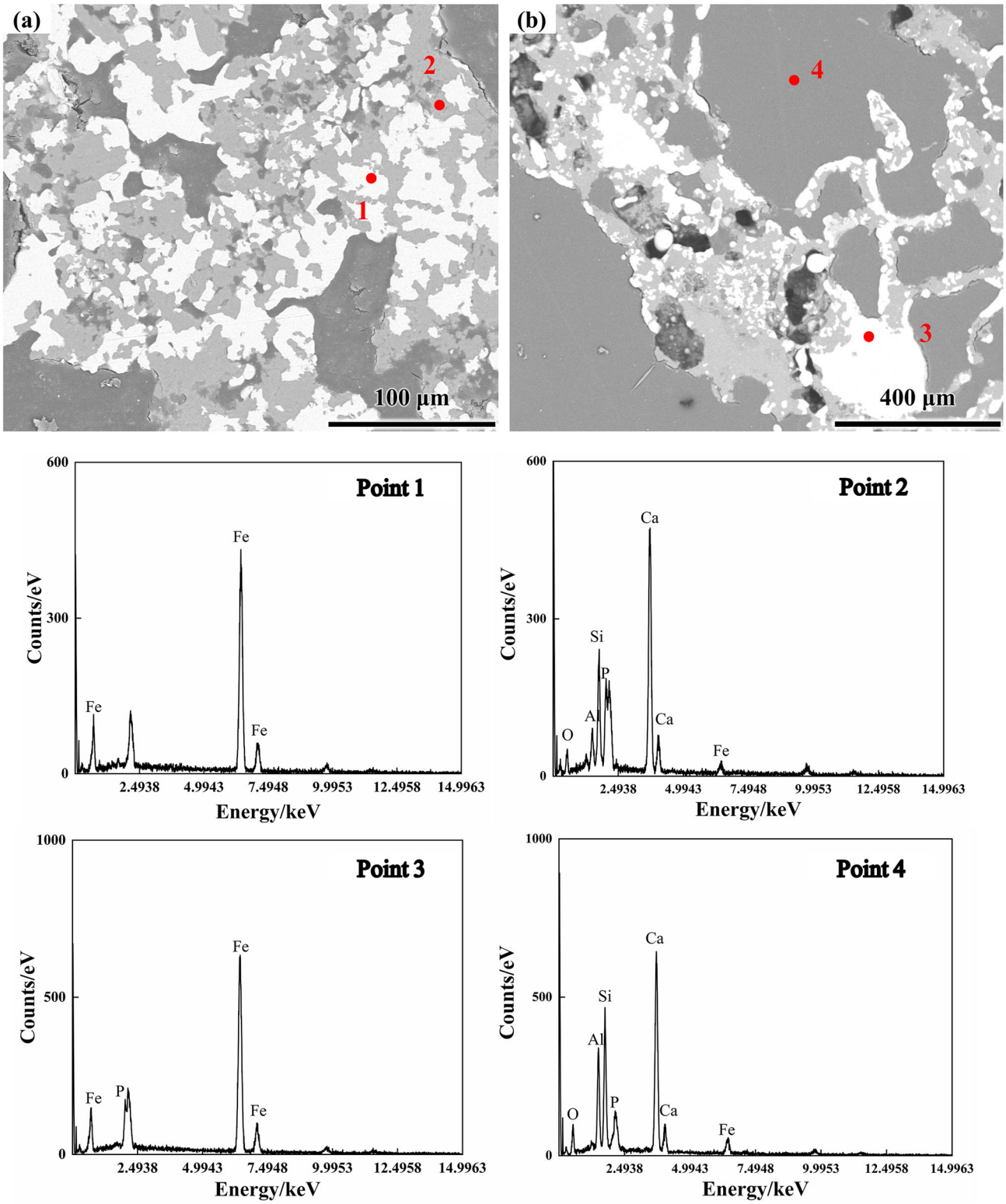

Fig. 9 Micromorphology of reduced pellets at different reduction time. **a** 1 h; **b** 4 h

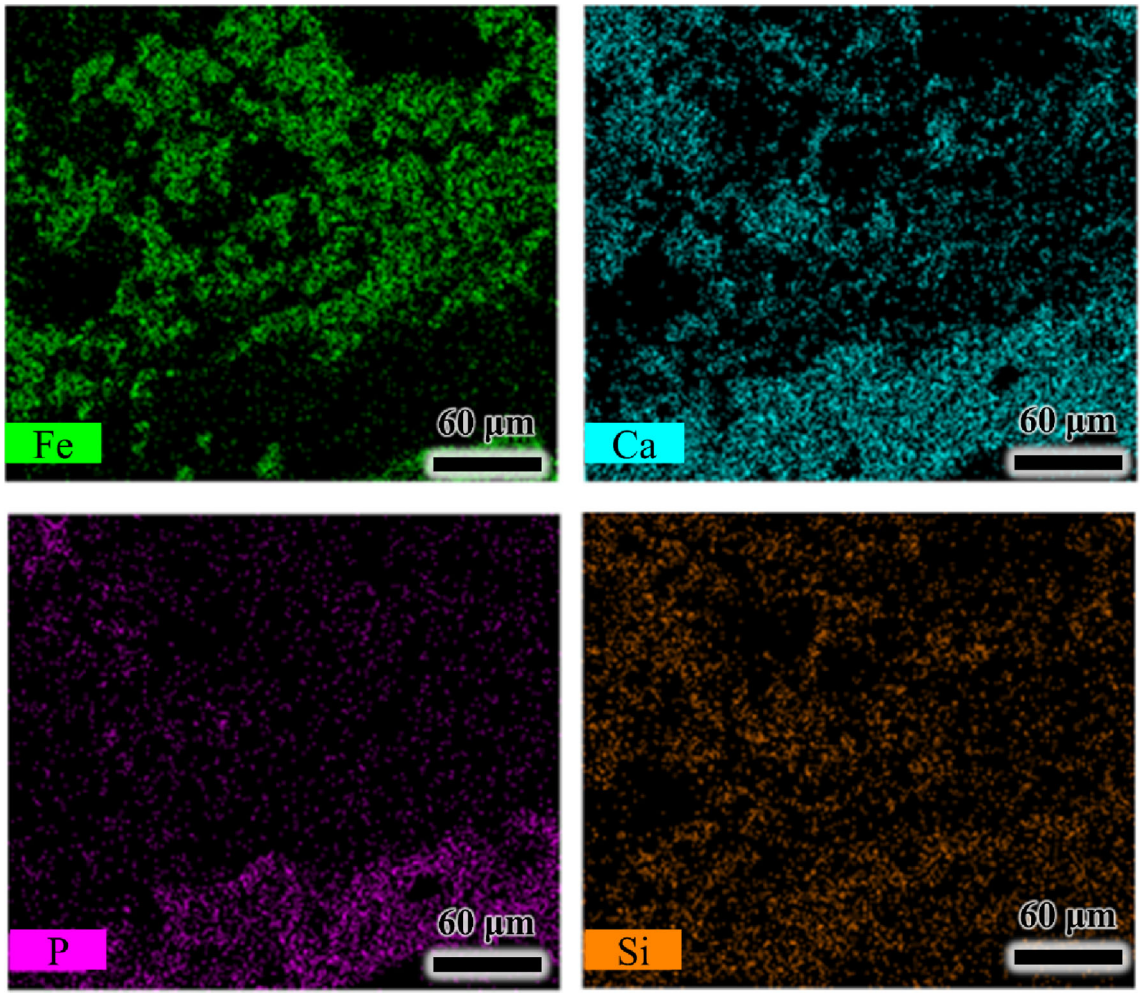

Fig. 10 Pellet surface scanning with reduction time of 1 h

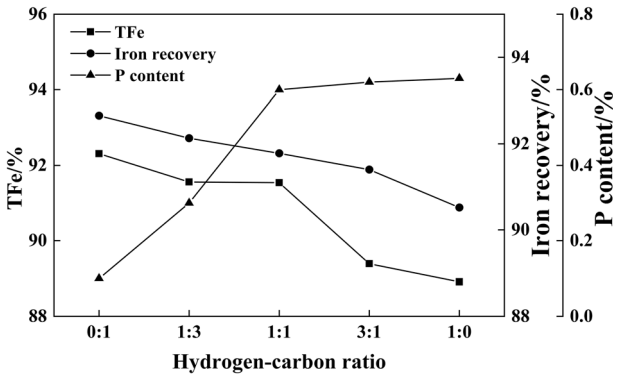

Fig. 11 Effects of hydrogen–carbon ratio on separation indices

and the diffraction peak of phosphorus at point 4 is lower than that of point 2, indicating that apatite is reduced with the increase in reduction time. In Fig. 10, P is highly overlapped with Ca while it has obvious boundary with Fe. This indicates that P still exists in apatite after 1 h reduction. Therefore, the optimal reduction time is 1 h.

3.3 Effect of hydrogen–carbon ratio

During the high-temperature reduction, the effects of CO and H_2 on the reduction process may differ [26]. To investigate the effects of varying hydrogen–carbon ratios on the reduction process and iron–phosphorus separation indices, the following fixed conditions were employed: 1100 °C, 4 L/min, 1 h, and 25% $CaCO_3$ addition. The experimental results are presented in Fig. 11.

When the hydrogen–carbon ratio increases, both the iron recovery and TFe decreased gradually while the phosphorus content increased significantly. The reason for the decrease in iron recovery and TFe may be that the oolitic structure is not destroyed and the size of iron particles is small. Figure 9a shows that the oolitic structure is destroyed and the iron particle size is large, when the reducing gas is CO. However, there is obvious oolitic structure in Fig. 12 when the hydrogen–carbon ratio is 1:1 and 1:0 (pure H_2). The main reason for the increase in phosphorus content may be that the oolitic structure is not

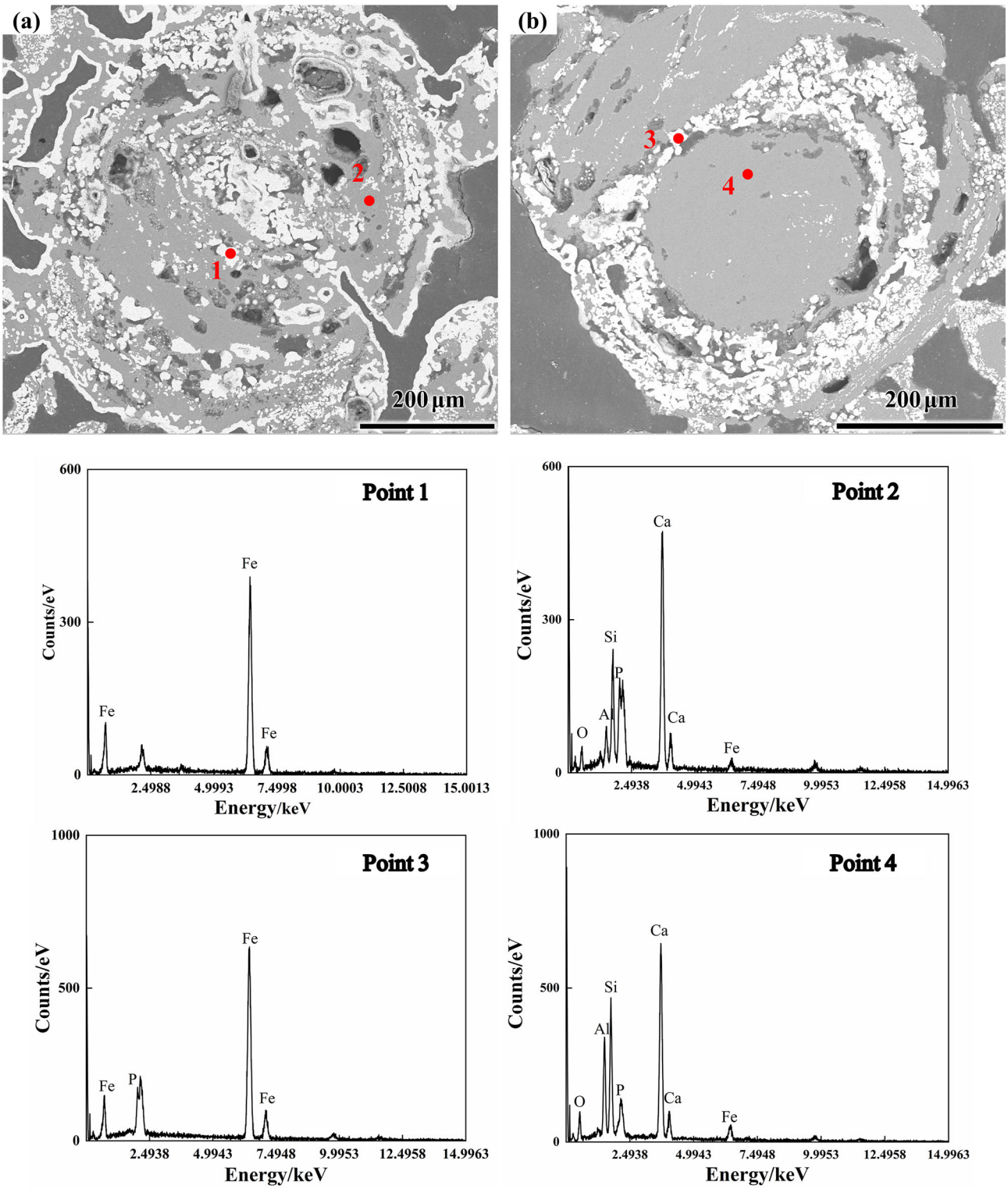

Fig. 12 Micromorphology of reduced pellets at different hydrogen–carbon ratios. **a** 1:1; **b** 1:0

destroyed and the apatite is reduced. Through the point scan results of point 3 in Fig. 12b, it can be found that there is phosphorus in metallic iron, while the result at point 1 is opposite. It can be seen from Fig. 13 that there are some overlapping parts of Fe and P when the hydrogen–carbon ratio is 1:0 (pure H_2). And compared with Fig. 7e, f, it is found that the diffraction peak of apatite disappears when

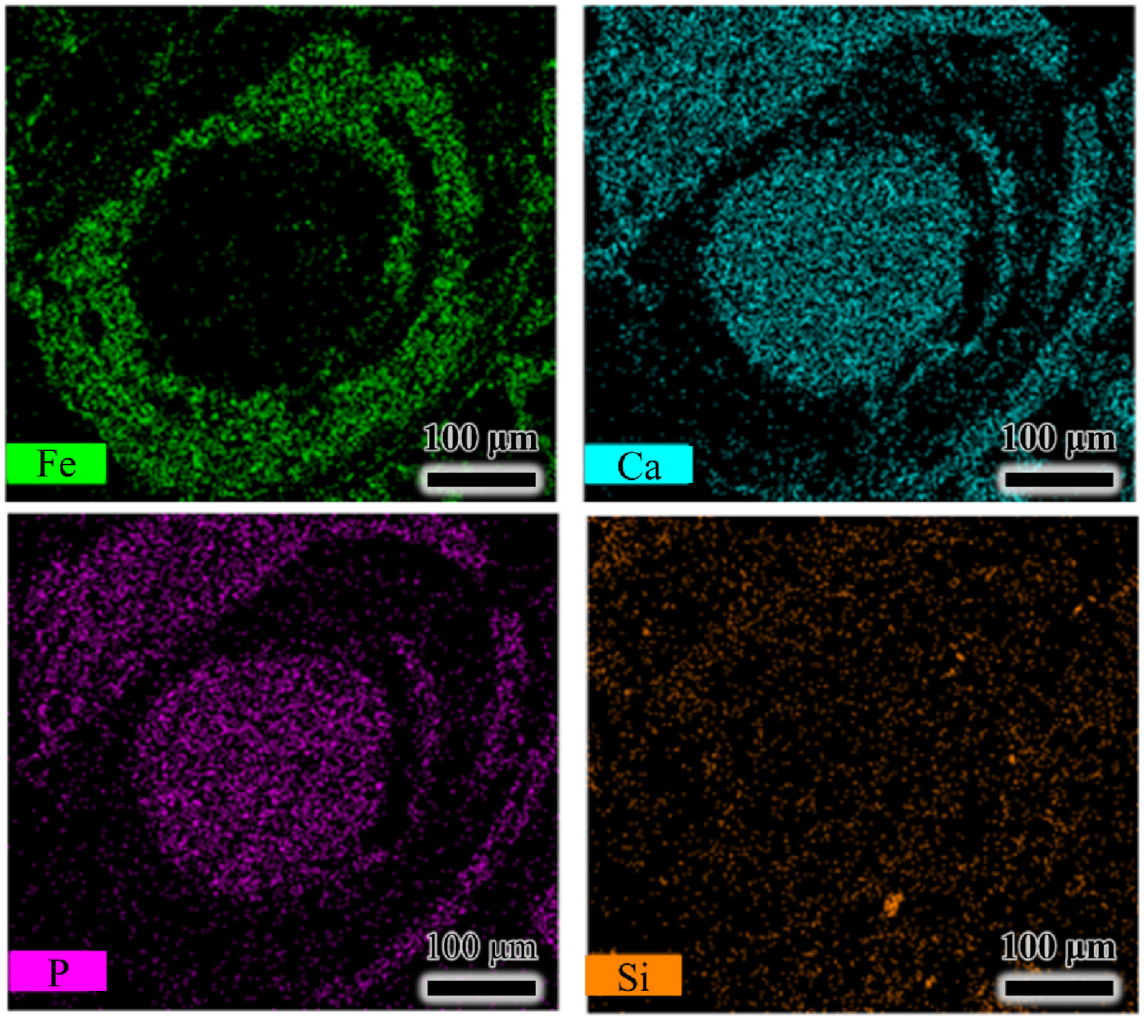

Fig. 13 Pellet surface scanning diagram with hydrogen–carbon ratio of 1:0 (pure H_2)

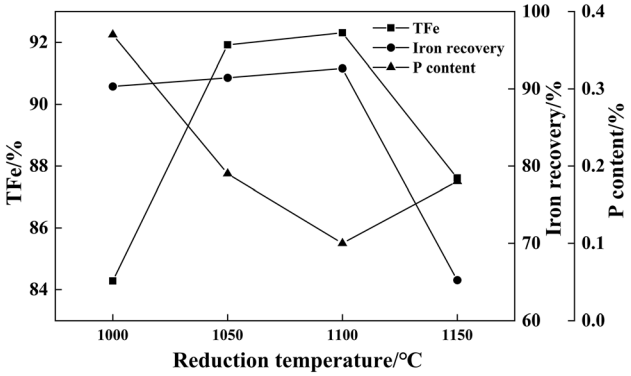

Fig. 14 Effects of reduction temperature on separation indices

the hydrogen–carbon ratio is 1:0 (pure H_2). This can prove that the phosphorus ash is reduced.

Increasing the proportion of H_2 in the reduction gas will lead to a smaller size of iron particles. H_2 has better reduction kinetics due to its smaller molecule and stronger diffusion capacity than CO. It is conducive to H_2 combination with minerals, so that the reduction efficiency is better [27]. At the same time, H_2 will inhibit the formation and extension of iron whiskers because its reduction is an endothermic reaction, thus hindering the growth of iron particles. As a result, some iron minerals with fine particle size are difficult to aggregate and grow after reduction when the oolitic structure is not completely destroyed. The small iron particles are not favorable for the recovery of iron in the magnetic field, resulting in the decrease in iron recovery as the hydrogen–carbon ratio increases. These small particles metallic iron mixed with gangue are difficult to be separated during the grinding magnetic separation process, resulting in the increase in phosphorus content and the decrease in TFe.

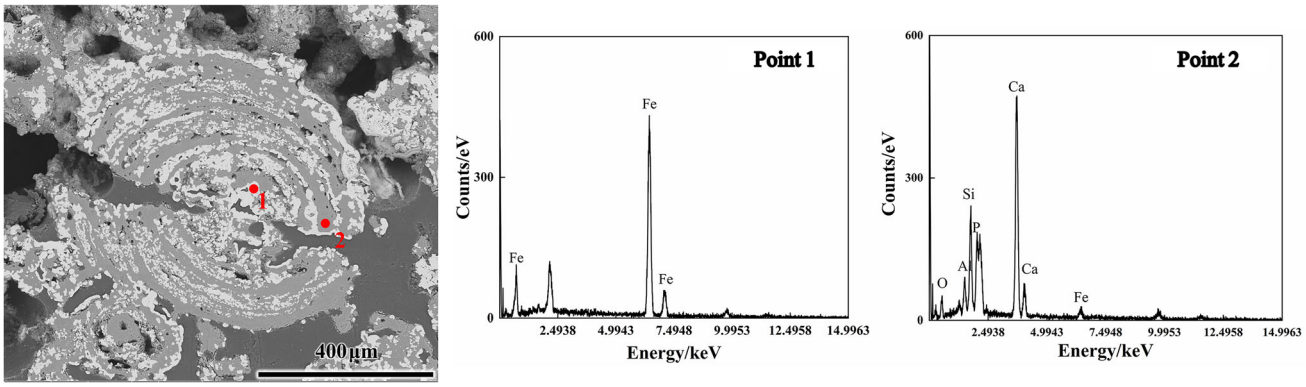

Fig. 15 Microscopic morphology of reduced pellets at 1000 °C

3.4 Effects of reduction temperature

Previous study has shown that the reduction temperature has a significant effect on the reduction process, and the reduction mechanism may be different at different reduction temperatures [28]. Generally, the increase in temperature can promote the reduction of iron oxides and is also beneficial to the formation and growth of metallic iron particles [29, 30]. To investigate the effect of different reduction temperatures on TFe, recovery rate and phosphorus content of directly reduced iron, other conditions were fixed at 4 L/min, 1 h, 25% $CaCO_3$, and the reducing gas is CO. The experimental results obtained are shown in Fig. 14.

The iron recovery gradually increases to 92.65% with the increase in reduction temperature and then suddenly decreases to 65.23% at 1150 °C. The phosphorus content decreases to its minimum of 0.10% at the reduction temperature of 1100 °C and increases when the reduction temperature increases. TFe increases from 84.28% at 1000 °C to 92.31% at 1100 °C and then decreases to 87.61% at 1150 °C.

At the reduction temperature of 1000 °C, the undamaged oolitic structure can be seen in Fig. 15. There is no phosphorus in metallic iron from the point scan results of point 1, indicating that apatite is not reduced. As can be seen from Fig. 9a, the oolitic structure is completely destroyed when the reduction temperature increases to 1100 °C. The boundary between large size metallic iron and gangue phase is obvious. It can be seen that the increase in the destroyed oolitic structure and the increase in iron particles lead to the increase in iron recovery and TFe and the decrease in phosphorus content when temperature increases from 1000 to 1100 °C. At the reduction temperature of 1150 °C, wustite and kirschsteinite are found in Fig. 7d. The results of point 3 in Fig. 16 show that there are wustite in the inner part of the pellets, indicating that the iron minerals in the pellets are not completely reduced. The iron particles in the inner parts are obviously smaller than those in the outer part. It can be seen from Fig. 17 that the boundary between iron and phosphorus is not clear and their distributions are complicated. The incomplete reduction of iron minerals and the small particle size of iron in the pellets result in the decrease in iron recovery and TFe, as well as the increase in phosphorus content.

According to the above results, it can be found that the process of reducing pellets by reducing gas conforms to the unreacted core model, and the pellets are gradually reduced from the outside to the inside. The newly formed metallic iron and low melting point gangue melt at the pellet boundary when the reduction temperature is too high. The reduction conditions inside pellets become worse because the reduction gas is blocked from entering the pellet, and the speed of $Fe_2O_3 \rightarrow Fe_3O_4 \rightarrow FeO \rightarrow Fe$ slows down, which is bad for the reduction of iron minerals and the growth of iron particles.

3.5 Discussion

The iron recovery mostly depends on the extent of iron mineral reduction, and the key factor is the complete conversion of iron minerals to metallic iron. The second factor is the size of the iron particles. Larger iron particles facilitate their separation in magnetic separation. The process of reducing phosphate-containing minerals (specifically apatite in this study) and the subsequent separation effect of iron and phosphorus using magnetic separation significantly affect the phosphorus content. When exposed to gangue substances like SiO_2 and Al_2O_3, apatite is easier to be reduced. Furthermore, the presence of additional dephosphorization agents can react with apatite to counteract the stimulating impact of gangue on its reduction [31–33]. By precisely regulating the reducing environment, the iron particles can attain a specific particle size (typically 20 μm) while the apatite is not reduced. This facilitates the separation of metallic iron particles from the

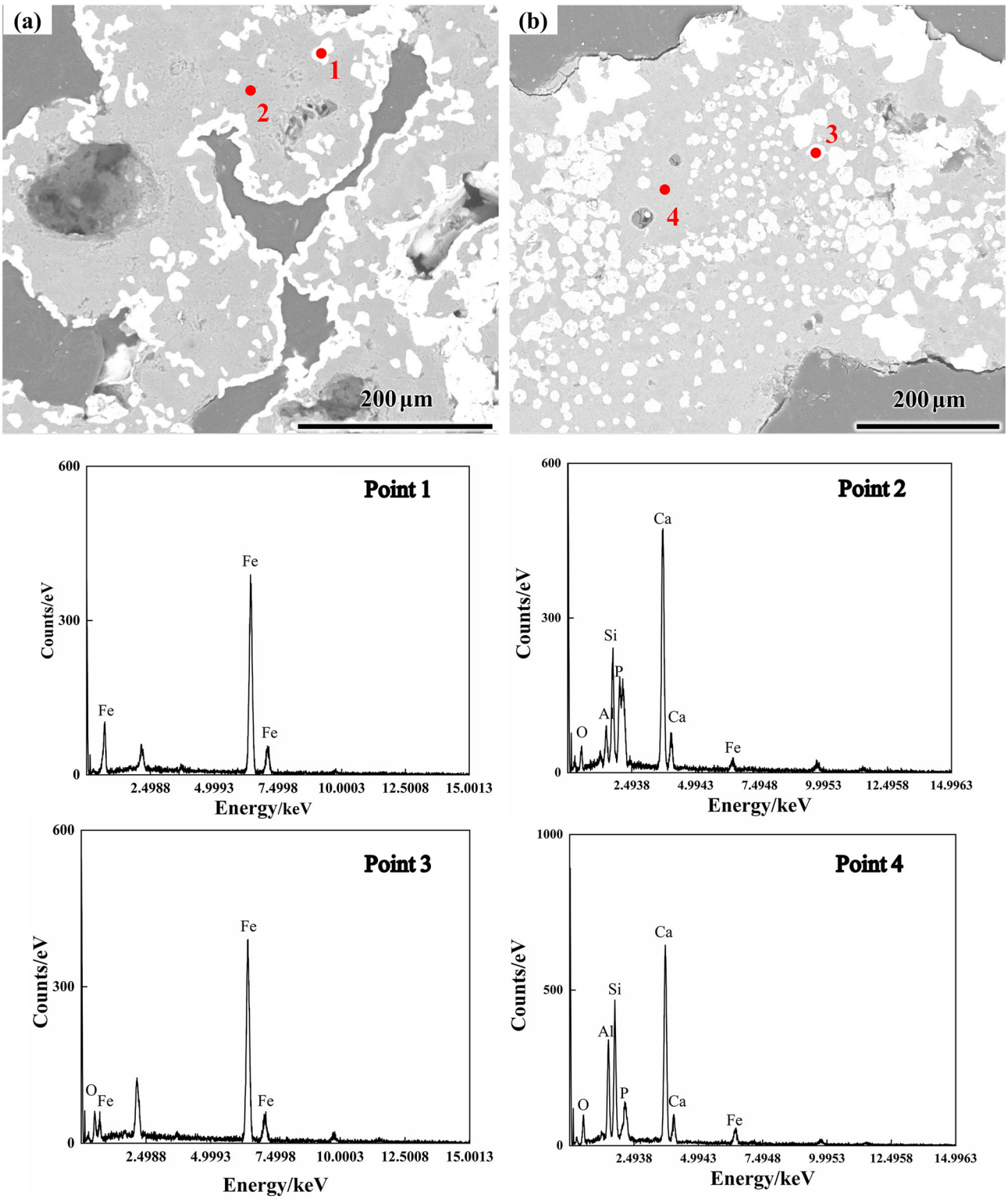

Fig. 16 Microscopic morphology of reduced pellets at 1150 °C. **a** Boundary; **b** interior

gangue during grinding magnetic separation. The separation of iron and phosphorus, as well as the phosphorus content in magnetic separation significantly affect the TFe. If apatite is not reduced, the dephosphorization agent will destroy the oolitic structure, facilitate the growth of iron particles, and promote the separation of iron particles from gangue [34].

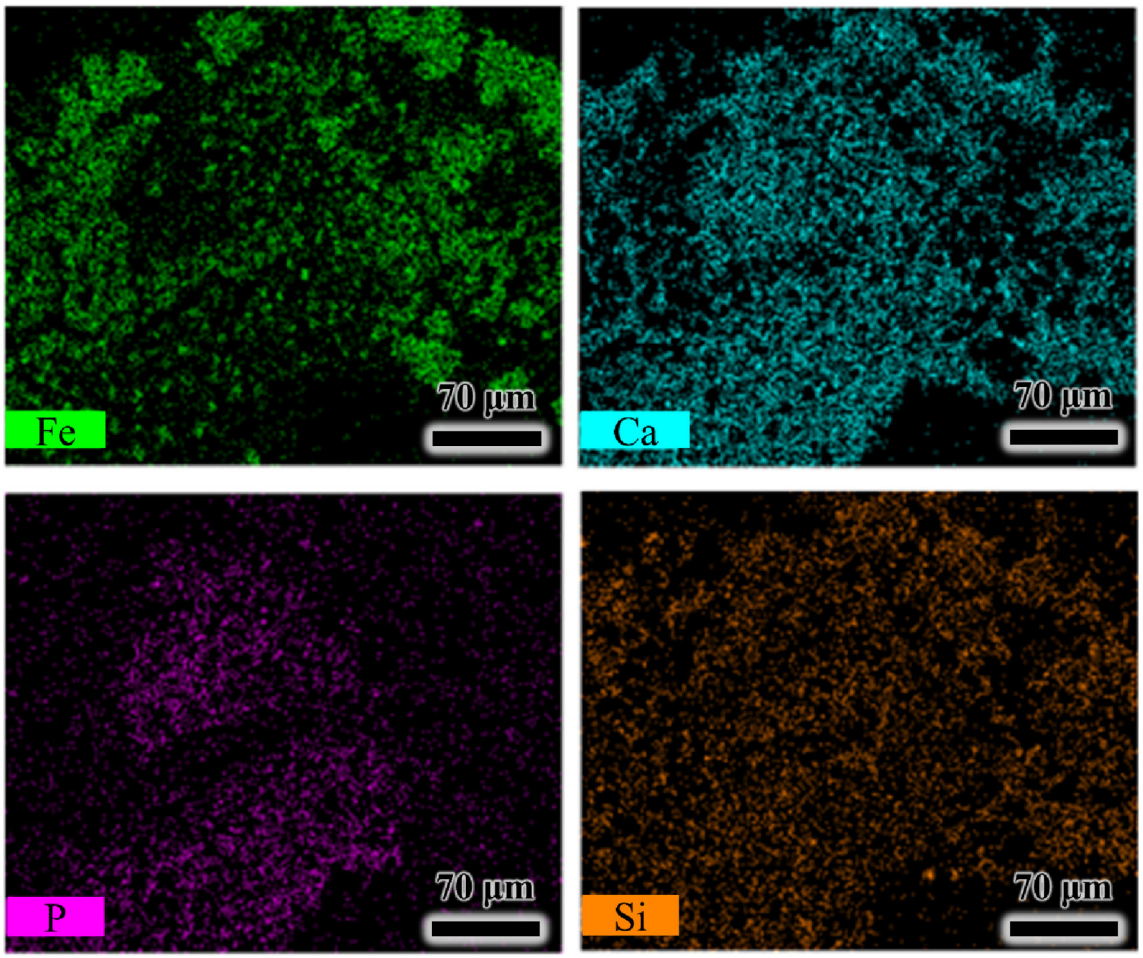

Fig. 17 Surface scanning of pellet interior of pellet at reduction temperature of 1150 °C

It is important to note that this study utilizes gas-based reduction instead of coal-based reduction. Prolonged gas-based reduction can result in a significant rise in apatite reduction. During the coal-based reduction process, the reducing atmosphere steadily diminishes with the consumption of coal. Conversely, in the gas-based reduction process, the reducing atmosphere remains constant. During the initial phases of gas-based reduction, iron oxide and apatite are engaged in a competitive interaction with the reducing gas. Apatite is easier to be reduced as the iron oxide level decreases. Therefore, during the gas-based reduction process, the duration of reduction significantly affects the phosphorus content.

4 Conclusions

1. The optimal parameters are found for the iron recovery and dephosphorization, which are the reduction temperature of 1100 °C, reduction time of 60 min, a CO flow rate of 2.8 L/min and N_2 flow rate of 1.2 L/min. The TFe and P contents of the obtained reduced iron are 92.31% and 0.10%, respectively, and the iron recovery is as high as 92.65%. This also proves the good feasibility of the proposed method in the study.
2. The reducing gas flow rate has a significant effect on iron recovery. Iron particles will be formed at relatively high reducing gas flow rate, which is beneficial to the growth of iron particles and further helps to increase the iron recovery.
3. When the reduction time increases, most hematite will be reduced to metallic iron in the beginning. However, apatite will also be reduced to P_2 with a longer reduction time, which further results in the inclusion of phosphorus in the metallic iron. Therefore, the reduction time should be controlled at the position where most hematite but less apatite is reduced.
4. When the hydrogen–carbon ratio increases, more H_2 will limit the formation and growth of iron whiskers and less destruction of oolitic structure, which results in the decrease in TFe and iron recovery but the increase in phosphorus. Therefore, less H_2 or pure CO

is helpful for the iron recovery and dephosphorization from HPOH.

5. Increasing the reduction temperature appropriately is beneficial to the growth of iron particles, and the separation effect of iron and phosphorus is good. However, if the reduction temperature is too high, the increase in the liquid phase will block the gas channel, making it difficult to completely reduce the iron ore inside the pellet. Therefore, the proper reduction temperature is found to be 1100 °C.

Acknowledgements This work was supported by the National Key R&D Program of China (Grant Nos. 2021YFC2902400 and 2021YFC2902404) and Interdisciplinary Research Project for Young Teachers of USTB (Fundamental Research Funds for the Central Universities) (FRF-IDRY-21-027 and FRF-IDRY-22-018).

Declarations

Conflict of interest The authors have no competing interests to declare that are relevant to the content of this article.

References

[1] S.K. Roy, D. Nayak, S.S. Rath, Powder Technol. 367 (2020) 796–808.
[2] S.U. Ofoegbu, Sustainability 11 (2019) 6787.
[3] K. Quast, Miner. Eng. 126 (2018) 89–100.
[4] Y. Sun, W. Zhou, Y. Han, Y. Li, Metals 9 (2019) 923.
[5] H.Q. Tang, J.W. Wang, Z.C. Guo, T. Ou, J. Iron Steel Res. Int. 20 (2013) No. 5, 17–23.
[6] D.B. Huang, Y.B. Zong, R.F. Wei, W. Gao, X.M. Liu, J. Iron Steel Res. Int. 23 (2016) 874–883.
[7] L. Guo, J.T. Gao, S.P. Zhong, Z.C. Guo, J. Iron Steel Res. Int. 26 (2019) 113–122.
[8] H.Q. Tang, Z.C. Guo, Z.L. Zhao, J. Iron Steel Res. Int. 17 (2010) No. 9, 1–6.
[9] W.T. Xia, Z.D. Ren, Y.F. Gao, J. Iron Steel Res. Int. 18 (2011) No. 5, 1–4.
[10] S. Mishra, S. Panda, A. Akcil, S. Dembele, Miner. Process. Extr. Metall. Rev. 44 (2023) 22–51.
[11] H. Zhang, P. Zhang, F. Zhou, M. Lu, Int. J. Min. Sci. Technol. 32 (2022) 865–876.
[12] D. Wang, J. Pan, D. Zhu, Z. Guo, C. Yang, Z. Yuan, J. Mater. Res. Technol. 19 (2022) 4296–4307.
[13] A. Yehia, S. Abd El-Halim, H. Sharada, M. Fadel, M. Ammar, Miner. Eng. 167 (2021) 106903.
[14] L. Zhang, R. Machiela, P. Das, M. Zhang, T. Eisele, Hydrometallurgy 184 (2019) 95–102.
[15] H. Zhang, Z. Zhang, L. Luo, H. Yu, Energy Sources, Part A: Recovery, Utilization, and Environmental Effects 41 (2019) 47–64.
[16] Y.S. Sun, Y.X. Han, P. Gao, Z.H. Wang, D.Z. Ren, Int. J. Miner. Metall. Mater. 20 (2013) 411–419.
[17] Y.S. Sun, Y.X. Han, P. Gao, D.Z. Ren, Int. J. Miner. Metall. Mater. 21 (2014) 331–338.
[18] H.Q. Tang, Y.Q. Qin, T.F. Qi, Z.L. Dong, Q.G. Xue, J. Iron Steel Res. Int. 23 (2016) 109–115.
[19] D.Q. Zhu, T.J. Chun, J. Pan, L.M. Lu, Z. He, Int. J. Miner. Metall. Mater. 20 (2013) 505–513.
[20] W. Yu, T. Sun, Z. Liu, J. Kou, C. Xu, ISIJ Int. 54 (2014) 56–62.
[21] Y.S. Sun, Y.F. Li, Y.X. Han, Y.J. Li, Int. J. Miner. Metall. Mater. 26 (2019) 938–945.
[22] W. Yu, Q.Y. Tang, J.A. Chen, T.C. Sun, Int. J. Miner. Metall. Mater. 23 (2016) 1126–1132.
[23] S.C. Wu, Z.Y. Li, T.C. Sun, J. Kou, X.H. Li, Int. J. Miner. Metall. Mater. 28 (2021) 1908–1916.
[24] S. Wu, T. Sun, J. Kou, E. Gao, Process Saf. Environ. Prot. 176 (2023) 304–315.
[25] S. Wu, T. Sun, J. Kou, H. Xu, Powder Technol. 413 (2023) 118043.
[26] K. Ma, J. Deng, G. Wang, Q. Zhou, J. Xu, Int. J. Hydrogen Energy 46 (2021) 26646–26664.
[27] L. Yi, Z. Huang, T. Jiang, L. Wang, T. Qi, Powder Technol. 269 (2015) 290–295.
[28] Z. Guo, D. Zhu, J. Pan, F. Zhang, J. Clean. Prod. 187 (2018) 910–922.
[29] H.H. Wang, G.Q. Li, D. Zhao, J.H. Ma, J. Yang, Hydrometallurgy 171 (2017) 61–68.
[30] Y. Li, T. Sun, J. Kou, Q. Guo, C. Xu, Miner. Process. Extr. Metall. Rev. 35 (2014) 66–73.
[31] J.W. Cha, D.Y. Kim, S.M. Jung, Metall. Mater. Trans. B 46 (2015) 2165–2179.
[32] W. Yu, T. Sun, J. Kou, Y. Wei, C. Xu, Z. Liu, ISIJ Int. 53 (2013) 427–433.
[33] C. Cheng, Q. Xue, G. Wang, Y. Zhang, J. Wang, Metall. Mater. Trans. B 47 (2016) 154–163.
[34] G. Li, S. Zhang, M. Rao, Y. Zhang, T. Jiang, Int. J. Miner. Process. 124 (2013) 26–34.

Springer Nature or its licensor (e.g. a society or other partner) holds exclusive rights to this article under a publishing agreement with the author(s) or other rightsholder(s); author self-archiving of the accepted manuscript version of this article is solely governed by the terms of such publishing agreement and applicable law.